Research Article | Vol. 31, No. 25 / 4 Dec 2023 / Optics Express 42667
Optics EXPRESS

Lagging propagation phase of spatially structured beams

ZHENYU WAN,[1,2,3,4,†] ZIYI TANG,[1,2,3,†] AND JIAN WANG[1,2,3,*]

[1]Wuhan National Laboratory for Optoelectronics and School of Optical and Electronic Information, Huazhong University of Science and Technology, Wuhan 430074, Hubei, China
[2]Optics Valley Laboratory, Wuhan 430074, Hubei, China
[3]Shenzhen Institute of Huazhong University of Science and Technology, Shenzhen 518000, China
[4]School of Physics and Astronomy, University of Glasgow, Glasgow G12 8QQ, UK
[†]These authors contributed equally to this work.
[*]jwang@hust.edu.cn

Abstract: The structured beams especially with spatially varying phase distribution have attracted tremendous attention in both physics and engineering. Recently, studies have shown that the transverse spatial confinement of optical fields or photons leads to a modification of the group velocity but the phase velocity of propagating structured beams is revealed insufficiently in the experiments. In this work, we provide the theoretical model and experimental observation of propagation phase of structured beams. The analysis suggests that the spatially structured beams with a definite axial component of wavevector k_r carry a so called "lagging propagation phase", which can be considered as a generalized Gouy phase that originally appears within a focal region. Taking the higher-order Bessel beam as an example, the propagation phase difference is demonstrated by mapping to the rotating angle of intensity patterns superposed with different radial and angular phase gradients. Physically, the lagging propagation phase may provide an interpretation for the dynamic evolution of complex structured beams or interfering fringes upon propagation such as the vortex knots or braids. From the application aspect, the lagging propagation phase would facilitate a promising way for structured beams in optical sensing and metrology.

1. Introduction

The propagation speed of light is a fundamental parameter in physics. Generally, the phase and group velocities are introduced to characterize the propagation speed of beams, where the phase velocity is attributed to the phase front [1]. For a plane wave with homogeneous phase distribution, it travels at the phase velocity of constant c in vacuum. As the wavefront shaping technique is developed rapidly in recent years [2,3], the optical fields have been customized with a variety of spatial phase structures, such as the nondiffracting Bessel beams [4,5], the Laguerre-Gaussian (LG) beams with orbital angular momentum (OAM) [6–8], and even an optical speckle with random-statistical properties [9,10]. Such beams have attracted great attention in many fields including optical trapping [11,12], imaging [13–16], sensing [17–20], communications [21–23], and quantum information [24–27]. When light beams are manipulated with complex transverse structures, the axial component of wavevector k_r is modified because wavefront curvature leads to a radial phase dependence. Recently, Giovannini *et al.* have observed a reduction in the group velocity of photons by imposing spatial confinement on them [28]. This phenomenon that the light beams or photons sculpted with spatial structures travel slower than the speed of light is called structured slowing effect and has brought great interest due to its profound implications. Subsequently, numerical and experimental studies have demonstrated the structured slowing effect with Bessel-Gaussian (BG) beams [29,30], LG beams [31,32], twisted photons [33,34], and optical speckles [35].

#510341 https://doi.org/10.1364/OE.510341
Journal © 2023 Received 25 Oct 2023; revised 17 Nov 2023; accepted 17 Nov 2023; published 1 Dec 2023

Optics EXPRESS

The relationship between phase velocity v_ϕ and group velocity v_g of spatially structured beams is analogous to a hollow waveguide considering that both waveguide and free-space configuration have transverse boundary conditions. In a waveguide, the dispersion relationship is given by $k_g^2 + k_s^2 = k_0^2$, where k_0 is wavenumber of the wave in free space, k_g is the guide propagation constant (corresponding to longitudinal component k_z in free space), and k_s is associated with the cutoff frequency of modes (corresponding to transverse component k_r in free space). Under the condition that k_s is determined by the section size and refractive index of the waveguide, i.e., $\partial k_s/\partial\omega = 0$, the relation equation is derived as $v_\phi v_g = c^2$ [36]. This means that at a subluminal group velocity, the phase velocity of spatially structured beams would be superluminal. Nevertheless, it is still investigated insufficiently how the superluminal phase velocity causes the propagation dynamics of structured beams.

In this work, we study the effect of spatial confinement on the propagation phase of structured beams. The analysis suggests that the structured beams with a k-spectrum distributed within a certain region have superluminal phase velocity. With such property, we propose a concept of structured lagging propagation phase to describe the extra phase shift induced by transverse structures upon propagation. The structured lagging propagation phase can be regarded as a generalized Gouy phase, where the well-known Gouy phase originates from the spread of transverse momenta near a focal region [37,38], while the structured lagging phase can also be found in collimated or propagation-invariant areas. Taking the higher-order Bessel beam as a typical example, which carries both radial and angular phase gradients, we show that by superposing it with a Gaussian beam the structured lagging phase can be extracted from the rotating angle of the interfering fringes. Particularly, such beam rotating upon propagation can be represented with a geometric offset on the equator of a hybrid Poincaré sphere where Gaussian and Bessel beams are located at the two poles respectively. Physically, the structured lagging phase may provide an interpretation for the dynamic evolution of complex structured beams upon propagation such as the vortex knots or braids [39,40]. The effects considered here would facilitate potential applications in optical sensing and metrology with structured beams.

2. Concept and theory

The phase velocity is introduced to describe the phase difference between the vibrations observed at two different locations in a free plane wave. However, this description does not provide a clear intuition when considering a structured beam with a collection of plane waves each travelling at different angles, especially with a non-trivial phase structure. For that we use a traditional definition of phase velocity $v_\phi = c \cdot k_0/k_z$ and extend it for structured beams to obtain $v_\phi = c \cdot k_0/\langle k_z\rangle$, where $\langle k_z\rangle$ refers to the expectation value of longitudinal wavevector and $\langle k_z\rangle/k_0$ is the average projection angle of wavevector towards the propagation axis. From the point of view of Fourier optics, the transverse phase structures of beams contribute to a certain distributed k-spectrum in Fourier space, where one would find the transverse projected wavevector components. According to the projection of wavevector, the longitudinal component is modified as $\langle k_z\rangle = \sqrt{k_0^2 - \langle k_r^2\rangle}$. This means that the k_z gets a reduction depending on the distributed range of k-spectrum. The spatially average phase velocity is then given as

$$v_\phi = \frac{c}{\sqrt{1 - \langle k_r^2\rangle/k_0^2}}. \tag{1}$$

Since the k_r^2 of structured beams takes positive value, the phase velocity is predicted to be superluminal, leading to an extra phase shift upon propagation. After a propagation distance Δz the phase difference between the structured beam and an on-axial plane wave is

$$\Delta\varphi = (c/v_\phi - 1)k_0 \cdot \Delta z \simeq -\frac{\langle k_r^2\rangle}{2k_0} \cdot \Delta z, \tag{2}$$

Optics EXPRESS

where the paraxial approximation is used with first-order Taylor polynomial. This minus sign means that the phase difference is lagging. Numerically, the structured lagging propagation phase experienced by the average Fourier component, as expressed in Eq. (2), coincides with the Gouy phase experienced by the fundamental Gaussian beam going through the beam waist [41]. Considering the diversity of structured beams, the structured lagging phase here can be regarded as a generalized Gouy phase.

The structured lagging phase is visualized by taking Bessel beam as an example, as shown in Fig. 1, where three beams shaped with different radial phase gradients are compared. For a plane wave or a collimated Gaussian beam, the transverse phase is flat and the k-spectrum is concentrated at the centre. The radial phase gradient provides a simple ring in k-spectrum of Bessel beam, whose k_r is single valued. A cone angle α, defined as $\alpha = \sin^{-1}(k_r/k_0)$, is used to characterize the Bessel beam. The larger the cone angle the steeper the radial phase gradient, and then the propagation period of the conical wavefront along the z direction is stretched, leading to a greater lagging phase. From Eq. (2), the lagging propagation phase of Bessel beams is derived as

$$\Delta\varphi_{Bessel} = -\frac{\alpha^2 k_0}{2} \cdot \Delta z. \tag{3}$$

For the higher-order Bessel beams carrying OAM, the angular phase gradients would lead to the wavevector being skewed with respect to the beam axis but such skew contributes nothing to k_r. Considering the achievable generation methods for higher-order Bessel beams with finite energy, for example illuminating an axicon with an LG beam [42], the divergence of LG beams which is proportional to the OAM index ℓ would affect the k_r. However, the divergence angle is negligible when ℓ is small compared with the cone angle α [43]. As a result, it is ignored in the following analysis.

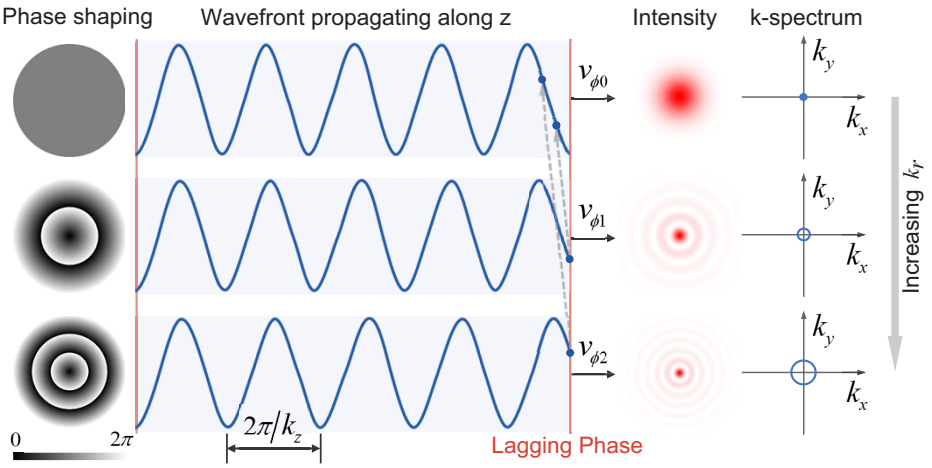

Fig. 1. Visualization of structured lagging propagation phase by comparing beams shaped with different radial phase gradients.

The phase difference between beams is usually extracted by using interference, with which the properties of Gouy phase are previously demonstrated. For example, in the case of superimposing Gaussian and radial LG beams, the destructive interference would give a dark beam focus surrounded by regions of higher intensity [44], and this is used to observe Gouy phase in quantum regime [45]. For superposed modes with different OAM indices or Rayleigh length parameters, the Gouy phase difference may form petal-like patterns that rotate about the beam axis as the beam passes through a focus or waist plane [46,47] or induce self-rotating polarization structures of hybrid vector beams [48,49]. Considering the interference between Gaussian and higher-order

Optics EXPRESS

Bessel beams, the structured lagging phase difference would lead to the superposed beam rotating upon propagation, as indicated in Fig. 2. The superposed beams are shaped like concentric petals, where the intensity variation on the circle of maximum energy density is written as

$$I(\phi, \Delta z)_{AC, r_{\max}} \sim \cos(\Delta\ell\phi - \Delta\alpha^2 k_0 \cdot \Delta z/2), \tag{4}$$

where ϕ is the polar angle, and $\Delta\ell$ is the OAM index difference. The rotating angle of a local intensity peak is then given as

$$\Delta\theta = \frac{\Delta\alpha^2 k_0 \cdot \Delta z}{2\Delta\ell}. \tag{5}$$

The orientation of superposed beam rotating along z is related to the sign of $\Delta\ell$. When the index is positive, the orientation is clockwise, as seen in Fig. 2(a); while the orientation becomes anticlockwise when the index is negative, as seen in Fig. 2(b). The rotation rate of a petal is proportional to the square of the cone angle. This is similar to the previous demonstration for rotation rate controlling by the difference in annular ring radius in Fourier plane of two superimposing Bessel beams [50]. For the case of multiple inner petals ($\Delta\ell > 1$), the three-dimensional trajectories of which appear like braided nodal lines [51]. The pitch of the braids, or in other words the propagation distance that the position of inner petals coincides with last one, is independent of the OAM index difference but to the cone angle. With a measured rotating angle, the structured lagging phase of a higher-order Bessel beam can be extracted by $\Delta\varphi_{Bessel} = -\Delta\theta \cdot \ell$.

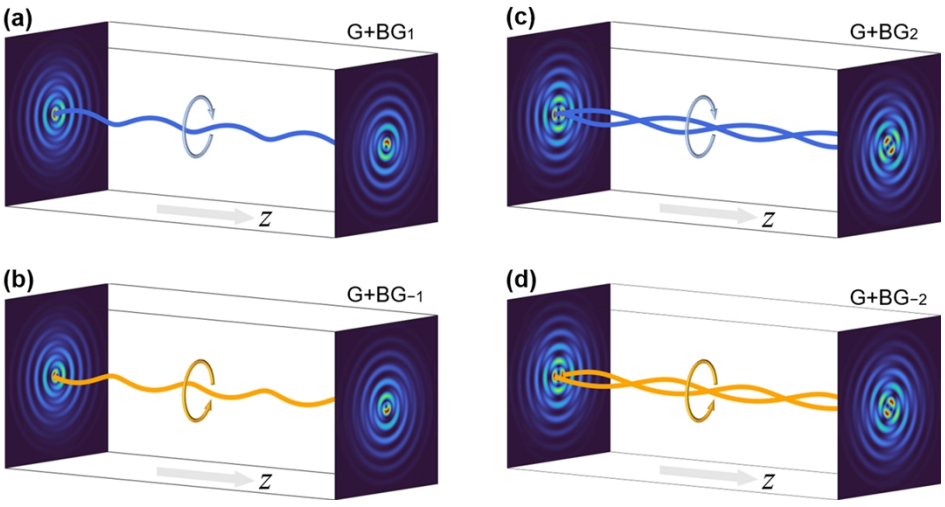

Fig. 2. Rotating beams upon propagation in free space induced by structured lagging phase difference between a Gaussian beam and a higher-order Bessel beam with (a) $\ell = 1$, (b) $\ell = -1$, (c) $\ell = 2$, (d) $\ell = -2$.

3. Experimental results

The experimental configuration for measuring the structured lagging propagation phase of higher-order Bessel beams is shown in Fig. 3. The laser at wavelength of 532 nm outputs a linearly-polarized Gaussian beam with diameter of about 0.75 mm. The beam is expanded through a 6× beam expander (BE) and is cleaned by the combination of two lenses ($f_1 = 50$ mm, $f_2 = 100$ mm) and a pinhole inserted at the focus. A half-wave plate (HWP) is employed to modify the polarization direction to match the working direction of the spatial light modulator

Optics EXPRESS

(SLM). The holographic patterns uploaded on SLM are designed in the same way as [52]. The SLM is calibrated in advance and its distortion is compensated with a conjugate phase. For a higher-order Bessel beam, the transverse phase function is $\ell\phi + \alpha k_0 \cdot r$, where $\ell\phi$ denotes an angular modulation to form OAM, $\alpha k_0 \cdot r$ refers to a radial modulation with an axicon phase gradient to modify the axial wavevector. After calculating the phase distribution of a superposed beam with different ℓ and/or α, a blazed diffraction grating along x is added on it to create the final phase-modulated hologram. With the grating, the first-order diffracted energy is angularly separated from the other orders, which are subsequently blocked using a spatial filter made up of a 4f system ($f_3 = f_4 = 400$ mm). A CCD (Mako G-223B) mounted at an electric translation stage (Thorlabs DDS300/M) moves from the imaging plane of SLM to observe the intensity distribution during propagation. The hologram generating and system controlling codes can be found in [53].

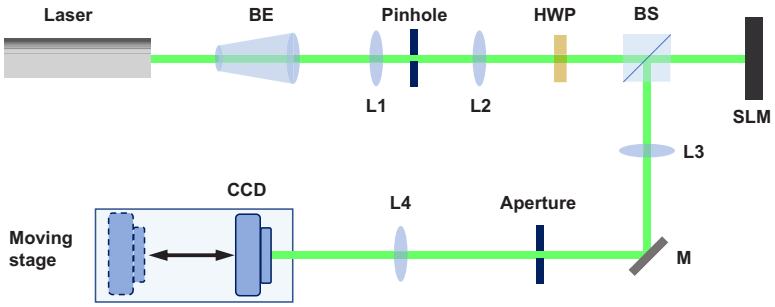

Fig. 3. Experimental setup for measuring the structured lagging propagation phase of higher-order Bessel beams. BE, beam expander; L1~L4, lens; HWP, half-wave plate; BS, beam splitter; SLM, spatial light modulator; M, mirror; CCD, charge coupled device.

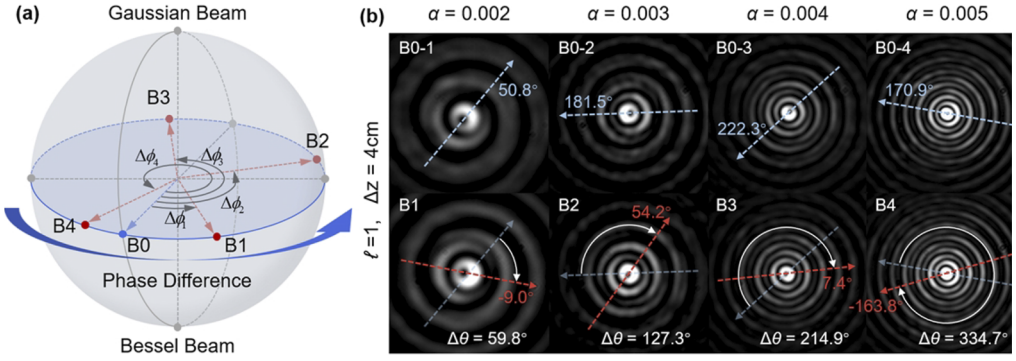

Fig. 4. The measured rotation angles of superimposing Gaussian beam and first-order Bessel beam after propagation. (a) The Poincaré sphere analogue to show the evolution of structured lagging phase difference during propagation. (b) Interfering intensity patterns captured between distance of 4 cm with different cone angles of Bessel beams, where B0-n corresponds to initial captures of Bn (n = 1, 2, 3, 4).

The rotation angles of superposed Gaussian beam and first-order Bessel beam with different cone angles after propagating through 4 cm are measured as shown in Fig. 4. The Poincaré sphere analogue provides a visual representation for studying the evolution of phase difference between two states [54,55]. With the Gaussian and Bessel beams as two poles of the sphere, the superposed beam is mapped onto the equator. Intuitively, determined by the structured lagging

Optics EXPRESS

phase difference, a geometric rotation occurs on the equator when the beam is propagating, as shown in Fig. 4(a). For a captured intensity pattern, the orientation of a petal is obtained by connecting beam axial position to the centroid of the petal (detailed codes can be found in [53]). Assigning the cone angle of Bessel beam from 0.002 to 0.005 with 0.001 interval, the measured rotation angles $\Delta\theta$ with propagation are 59.8°, 127.3°, 214.9°, 334.7° respectively, where the theoretical expected values from Eq. (5) are 54.1°, 121.8°, 216.5°, 338.3° respectively. Note that the rotational Doppler shift for light beams with OAM can be interpreted using the dynamic evolution on a Poincaré sphere analogue [54]. Similarly, when observing the propagation of the superposed Gaussian and Bessel beams over time, the location on the corresponding Poincaré sphere will move along the equator and then the time-varying phase difference would give rise to a Doppler beat signal.

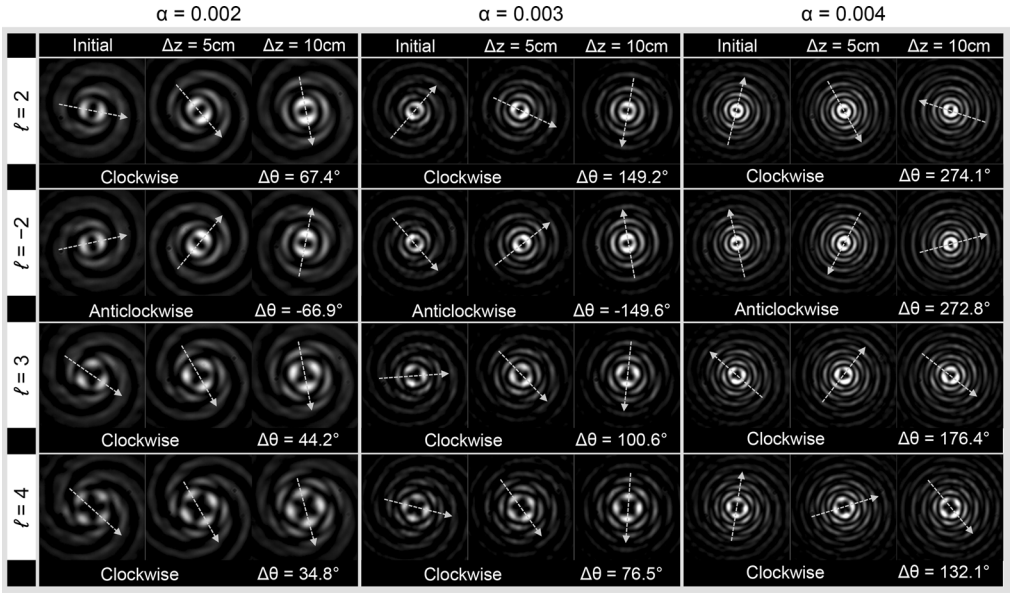

Fig. 5. The measured magnitude and orientation of rotation angles of superimposing Gaussian beam and higher-order Bessel beam after propagation. Columns and rows represent cases in which the Bessel beam has different cone angles ($\alpha = 0.002, 0.003, 0.004$) and OAM indices ($\ell = 2, -2, 3, 4$).

The results in Fig. 5 show the rotating angles of superposed Gaussian beam and higher-order Bessel beams at discrete distances, where each column and row correspond to a different cone angle α and OAM index ℓ of the Bessel beam. The number of petals on an inner annule is denoted by $|\ell|$. The orientation of the petals on the beams is characterized by connecting the beam axis with the centroid of any petal to be tracked. The beam axis is determined by the geometrical centre of centroid of all the inner petals. It can be seen that the direction of superposed beam rotating is related to the sign of ℓ, and the magnitude of rotation angle is reduced as $|\ell|$ increases while is enhanced with the increase of α. The measured rotation angles are in agreement as predicted by Eq. (5). A further demonstration is shown in Fig. 6 where the beams are superposed by two Bessel beams. The beams would propagate with the static intensity distribution when $\Delta\alpha = 0$. In the case that difference appears between the cone angles of the two Bessel beams, the orientation of beam rotating during propagation is reversed with the sign of $\Delta\ell$. Note that in both Figs. 4 and 5, the intensity of petals is slightly higher after propagating a short distance than the initial. This is because the generated Bessel beam is not ideal and the propagation-invariant region is restricted by the overlapping range of plane waves distributed conically.

Optics EXPRESS

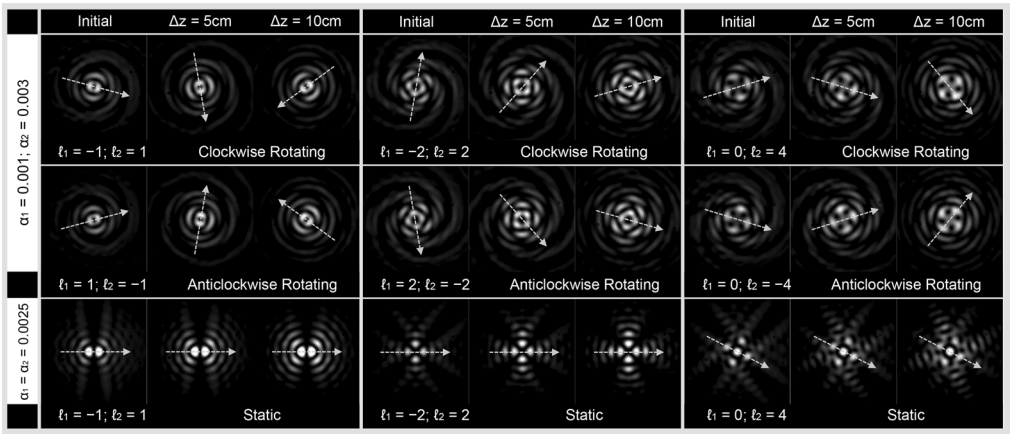

Fig. 6. The measured orientation of beam rotating during propagation with superposed two Bessel beams. The upper row shows the rotating orientation with different $\Delta\ell$ for the two Bessel beams having different cone angles ($\alpha_1 = 0.001$, $\alpha_2 = 0.003$). The lower row shows the static beam when the Bessel beams have the same cone angle ($\alpha_1 = \alpha_2 = 0.0025$).

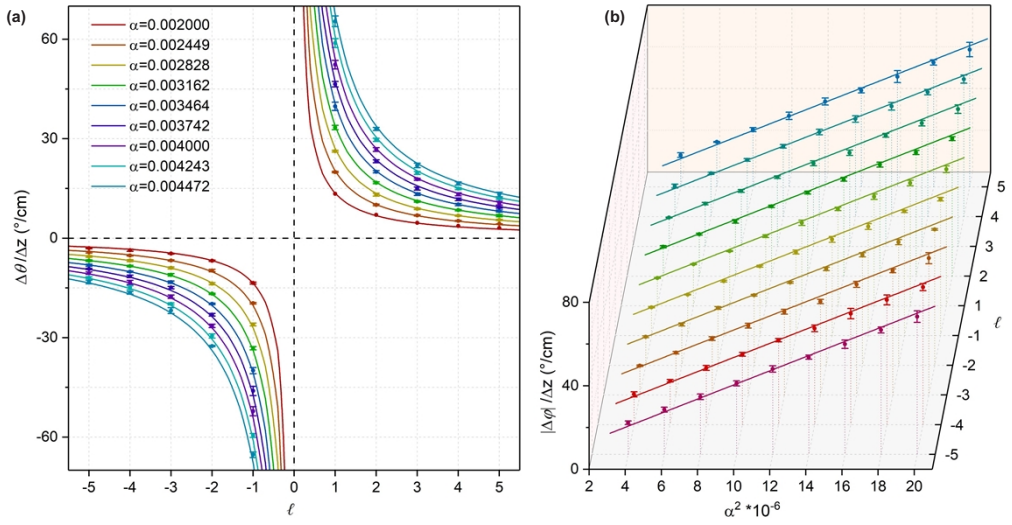

Fig. 7. (a) The measured radio of rotation angle to the propagation distance for superposed Gaussian and higher-order Bessel beams with diverse cone angles and OAM indices. (b) The radio of structured lagging phase difference to the propagation distance derived from (a).

Optics EXPRESS

For superposed Gaussian and higher-order Bessel beams with diverse cone angles and OAM indices we then measured the radio of beam rotating angle to the propagation distance to demonstrate the relationship between structured lagging phase and the indices α and ℓ, as shown in Fig. 7. The transverse structure of a superposed beam in k-space remains upon propagation, meaning that the rotating rate $\Delta\theta/\Delta z$ does not change with position. To obtain it, two frames 20 cm apart are captured for extracting the rotation angle and a video of beam propagating is recorded for determining the rotational orientation and the number of turns. In our strategy for processing the captured frames [53], the beam intensity is digitized to find the centroid of a petal, where the setting of gray-scale threshold would affect the final calculated results of the angle. The error bar in each data point is measured 5 times at different initial frame locations and the processing thresholds. The results in Fig. 7(a) indicate that the measured rotating rates match the theoretical curves by Eq. (5) quite well. This radio of structured lagging phase difference to the propagation distance as a function of cone angle can then be deduced for the rotating rates using the relation $\Delta\varphi_{Bessel} = -\Delta\theta \cdot \ell$. The phase changing rates are linearly correlated to the square of α, and parallel lines under different ℓ means that the phase changing rates are independent of ℓ. The structured lagging phase here is controlled by α rather than ℓ because only the radial phase gradient contributes to the spreading of k-spectrum. The k-spectrum of higher-order Bessel beams has the profile of perfect vortex beams [56], in which arbitrary topological charges share the same ring radius associated with α.

4. Discussions and conclusions

In this work, we have introduced and characterized the proposed concept of structured lagging propagation phase. Taking the higher-order Bessel beam as an example, the structured lagging phase is demonstrated and measured from the beam rotating angle during propagation by interfering with a Gaussian beam. Note that the rotation of intensity profiles observed here is distinct from the beam rotating upon propagation along a non-planar trajectory [57], where the former is induced by the spatial spreading of the k-spectrum or plane wave components while the latter is associated with the geometric phases. Considering the similarity between the physical origin between the structured lagging phase and the Gouy phase in terms of the transverse spatial confinement, it can be extended as the generalized Gouy phase in a collimated region. The structured lagging phase may provide a potential candidate for applying in optical sensing and metrology. For example, in previous studies [18,58], with the propagation properties of Bessel beams, some schemes have been demonstrated such as refractometer and displacement measurements.

On the other hand, the structured lagging phase may also provide an interpretation for the propagation evolution of structured beams with more complicated phase modulation. In the case that a higher-order Bessel beam is superposed with a Gaussian beam, the rotating rates during propagation are uniform; while with the same structured lagging phase difference, the rotating rates present angular acceleration and deceleration when the angular phase variation is modulated nonlinearly [59]. By interfering beams with different structured propagation phases, the spiraling beams have been observed recently enabling the accelerating trajectory over both radial and angular directions, for example, the monochromatic tornado beams created by superimposing ring-Airy beams [60] or swallowtail vortex beams [61,62]. Beyond that, with a group of structured lagging phases that are carefully designed with harmonic longitudinal wavevectors, the longitudinal structured beams can be created with 3D constructive and destructive interference, where for instance the intensity pattern of beam would be frozen within a certain distance region [63,64], enabling the probing of atmospheric turbulence strength distribution [65]. Fascinating propagation properties are revealed by customizing the transverse phase distribution and structured propagation phase of light fields, providing a useful tool in optical trapping and manipulations.

Optics EXPRESS

Funding. National Natural Science Foundation of China (62125503, 62261160388); Natural Science Foundation of Hubei Province (2023AFA028); Shenzhen Science and Technology Program (JCYJ20200109114018750); Innovation Project of Optics Valley Laboratory (OVL2021BG004).

Acknowledgments. We would like to acknowledge Prof. Miles J. Padgett at University of Glasgow for his fruitful discussions.

Disclosures. The authors declare no conflicts of interest.

Data availability. Data underlying the results presented in this paper may be obtained from the authors upon reasonable request and the MATLAB codes for data collection and processing are available online [53].

References

1. I. S. Grant and W. R. Phillips, *Electromagnetism*. (Wiley, 1980).
2. A. Forbes, A. Dudley, and M. McLaren, "Creation and detection of optical modes with spatial light modulators," Adv. Opt. Photonics **8**(2), 200–227 (2016).
3. S. Scholes, R. Kara, J. Pinnell, *et al.*, "Structured light with digital micromirror devices: a guide to best practice," Opt. Eng. **59**(04), 1 (2019).
4. D. McGloin and K. Dholakia, "Bessel beams: Diffraction in a new light," Contemp. Phys. **46**(1), 15–28 (2005).
5. M. Mazilu, D. James Stevenson, F. Gunn-Moore, *et al.*, "Light beats the spread: "non-diffracting" beams," Laser & Photon. Rev. **4**(4), 529–547 (2010).
6. L. Allen, M. W. Beijersbergen, R. J. C. Spreeuw, *et al.*, "Orbital angular momentum of light and the transformation of Laguerre-Gaussian laser modes," Phys. Rev. A **45**(11), 8185–8189 (1992).
7. S. Franke-Arnold, L. Allen, and M. J. Padgett, "Advances in optical angular momentum," Laser & Photon. Rev. **2**(4), 299–313 (2008).
8. M. J. Padgett, "Orbital angular momentum 25 years on [Invited]," Opt. Express **25**(10), 11265–11274 (2017).
9. N. Bender, H. Yılmaz, Y. Bromberg, *et al.*, "Customizing speckle intensity statistics," Optica **5**(5), 595–600 (2018).
10. R. Liu, B. Qing, S. Zhao, *et al.*, "Generation of non-Rayleigh nondiffracting speckles," Phys. Rev. Lett. **127**(18), 180601 (2021).
11. M. J. Padgett and R. Bowman, "Tweezers with a twist," Nat. Photonics **5**(6), 343–348 (2011).
12. Y. Yang, Y. Ren, M. Chen, *et al.*, "Optical trapping with structured light: a review," Adv. Photon. **3**(03), 034001 (2021).
13. F. O. Fahrbach, P. Simon, and A. Rohrbach, "Microscopy with self-reconstructing beams," Nat. Photonics **4**(11), 780–785 (2010).
14. C. Maurer, A. Jesacher, S. Bernet, *et al.*, "What spatial light modulators can do for optical microscopy," Laser & Photon. Rev. **5**(1), 81–101 (2011).
15. E. Mudry, K. Belkebir, J. Girard, *et al.*, "Structured illumination microscopy using unknown speckle patterns," Nat. Photonics **6**(5), 312–315 (2012).
16. J. Zeng, Y. Dong, Y. Wang, *et al.*, "Optical imaging using orbital angular momentum: interferometry, holography and microscopy," J. Lightwave Technol. **41**(7), 2025–2040 (2023).
17. M. P. J. Lavery, F. C. Speirits, S. M. Barnett, *et al.*, "Detection of a spinning object using light's orbital angular momentum," Science **341**(6145), 537–540 (2013).
18. A. H. Dorrah, M. Zamboni-Rached, and M. Mojahedi, "Experimental demonstration of tunable refractometer based on orbital angular momentum of longitudinally structured light," Light: Sci. Appl. **7**(1), 40 (2018).
19. Z. Wan, L. Fang, and J. Wang, "Direction-discriminated rotational Doppler velocimetry with circularly polarized vortex beams," Opt. Lett. **47**(5), 1021–1024 (2022).
20. Z. Zhi, Q. Na, Q. Xie, *et al.*, "On-chip generation of Bessel-Gaussian beam via concentrically distributed grating arrays for long-range sensing," Light: Sci. Appl. **12**(1), 92 (2023).
21. Z. Qiao, Z. Wan, G. Xie, *et al.*, "Multi-vortex laser enabling spatial and temporal encoding," PhotoniX **1**(1), 13 (2020).
22. J. Wang, J. Liu, S. Li, *et al.*, "Orbital angular momentum and beyond in free-space optical communications," Nanophotonics **11**(4), 645–680 (2022).
23. A. E. Willner, H. Song, K. Zou, *et al.*, "Orbital angular momentum beams for high-capacity communications," J. Lightwave Technol. **41**(7), 1918–1933 (2023).
24. J. Leach, B. Jack, J. Romero, *et al.*, "Quantum correlations in optical angle-orbital angular momentum variables," Science **329**(5992), 662–665 (2010).
25. M. Erhard, R. Fickler, M. Krenn, *et al.*, "Twisted photons: new quantum perspectives in high dimensions," Light: Sci. Appl. **7**(3), 17146 (2017).
26. J. Liu, I. Nape, Q. Wang, *et al.*, "Multidimensional entanglement transport through single-mode fiber," Sci. Adv. **6**(4), eaay0837 (2020).
27. E. Otte, I. Nape, C. Rosales-Guzmán, *et al.*, "High-dimensional cryptography with spatial modes of light: tutorial," J. Opt. Soc. Am. B **37**(11), A309–A323 (2020).
28. D. Giovannini, J. Romero, V. Potoček, *et al.*, "Spatially structured photons that travel in free space slower than the speed of light," Science **347**(6224), 857–860 (2015).
29. R. R. Alfano and D. A. Nolan, "Slowing of Bessel light beam group velocity," Opt. Commun. **361**(15), 25–27 (2016).

Optics EXPRESS

30. P. Saari, "Reexamination of group velocities of structured light pulses," Phys. Rev. A **97**(6), 063824 (2018).
31. F. Bouchard, J. Harris, H. Mand, *et al.*, "Observation of subluminal twisted light in vacuum," Optica **3**(4), 351–354 (2016).
32. N. D. Bareza and N. Hermosa, "Subluminal group velocity and dispersion of Laguerre Gauss beams in free space," Sci. Rep. **6**(1), 26842 (2016).
33. A. Lyons, T. Roger, N. Westerberg, *et al.*, "How fast is a twisted photon?" Optica **5**(6), 682–686 (2018).
34. F. Tamburini, B. Thidé, I. Licata, *et al.*, "Majorana bosonic quasiparticles from twisted photons in free space," Phys. Rev. A **103**(3), 033505 (2021).
35. Z. Wan, M. Yessenov, and M. J. Padgett, "The propagation speed of optical speckle," Sci. Rep. **13**(1), 9071 (2023).
36. W. K. H. Panofsky and M. Phillips, "*Classical Electricity and Magnetism*," (Addison-Wesley, 1962).
37. S. Feng and H. G. Winful, "Physical origin of the Gouy phase shift," Opt. Lett. **26**(8), 485–487 (2001).
38. Q. Zhan, "Second-order tilted wave interpretation of the Gouy phase shift under high numerical aperture uniform illumination," Opt. Commun. **242**(4-6), 351–360 (2004).
39. M. V. Berry and M. R. Dennis, "Knotted and linked phase singularities in monochromatic waves," Proc. R. Soc. Lond. A **457**(2013), 2251–2263 (2001).
40. A. A. Voitiv, J. M. Andersen, M. E. Siemens, *et al.*, "Optical vortex braiding with Bessel beams," Opt. Lett. **45**(6), 1321–1324 (2020).
41. T. Ackemann, W. Grosse-Nobis, and G.L. Lippi, "The Gouy phase shift, the average phase lag of Fourier components of Hermite–Gaussian modes and their application to resonance conditions in optical cavities," Opt. Commun. **189**(1-3), 5–14 (2001).
42. J. Arlt and K. Dholakia, "Generation of high-order Bessel beams by use of an axicon," Opt. Commun. **177**(1-6), 297–301 (2000).
43. M. J. Padgett, F. M. Miatto, M. P. J. Lavery, *et al.*, "Divergence of an orbital-angular-momentum-carrying beam upon propagation," New J. Phys. **17**(2), 023011 (2015).
44. J. Arlt and M. J. Padgett, "Generation of a beam with a dark focus surrounded by regions of higher intensity: the optical bottle beam," Opt. Lett. **25**(4), 191–193 (2000).
45. M. Hiekkamäki, R. F. Barros, M. Ornigotti, *et al.*, "Observation of the quantum Gouy phase," Nat. Photonics **16**(12), 828–833 (2022).
46. S. M. Baumann, D. M. Kalb, L. H. MacMillan, *et al.*, "Propagation dynamics of optical vortices due to Gouy phase," Opt. Express **17**(12), 9818–9827 (2009).
47. J. Webster, C. Rosales-Guzmán, and A. Forbes, "Radially dependent angular acceleration of twisted light," Opt. Lett. **42**(4), 675–678 (2017).
48. M. M. Sánchez-López, J. A. Davis, I. Moreno, *et al.*, "Gouy phase effects on propagation of pure and hybrid vector beams," Opt. Express **27**(3), 2374–2386 (2019).
49. P. Li, X. Fan, D. Wu, *et al.*, "Self-accelerated optical activity in free space induced by the Gouy phase," Photonics Res. **8**(4), 475 (2020).
50. R. Rop, A. Dudley, C. López-Mariscal, *et al.*, "Measuring the rotation rates of superpositions of higher-order Bessel beams," J. Mod. Opt. **59**(3), 259–267 (2012).
51. M. R. Dennis, "Braided nodal lines in wave superpositions," New J. Phys. **5**(1), 134 (2003).
52. J. Leach, G. M. Gibson, M. J. Padgett, *et al.*, "Generation of achromatic Bessel beams using a compensated spatial light modulator," Opt. Express **14**(12), 5581–5587 (2006).
53. Z. Wan and Z. Tang, in GitHub Repository, https://github.com/ZWan1/StructuredBeamMonitoring (2023).
54. M. J. Padgett and J. Courtial, "Poincare-sphere equivalent for light beams containing orbital angular momentum," Opt. Lett. **24**(7), 430–432 (1999).
55. J. Zhong, S. Liu, K. Wang, *et al.*, "Poincare sphere analogue for optical vortex knots," Opt. Lett. **47**(2), 313–316 (2022).
56. P. Vaity and L. Rusch, "Perfect vortex beam: Fourier transformation of a Bessel beam," Opt. Lett. **40**(4), 597–600 (2015).
57. A. McWilliam, C. M. Cisowski, R. Bennett, *et al.*, "Angular momentum redirection phase of vector beams in a non-planar geometry," Nanophotonics **11**(4), 727–736 (2022).
58. S. Prabhakar, S. Z. D. Plachta, M. Ornigotti, *et al.*, "High-accuracy longitudinal position measurement using self-accelerating light," Appl. Opt. **60**(11), 3203–3210 (2021).
59. C. Schulze, F. S. Roux, A. Dudley, *et al.*, "Accelerated rotation with orbital angular momentum modes," Phys. Rev. A **91**(4), 043821 (2015).
60. A. Brimis, K. G. Makris, and D. G. Papazoglou, "Tornado waves," Opt. Lett. **45**(2), 280–283 (2020).
61. Y. Zhang, J. Tu, S. He, *et al.*, "Experimental generation of the polycyclic tornado circular swallowtail beam with self-healing and auto-focusing," Opt. Express **30**(2), 1829–1840 (2022).
62. J. Jiang, D. Xu, Z. Mo, *et al.*, "Generation and control of tornado waves by means of ring swallowtail vortex beams," Opt. Express **30**(7), 11331–11344 (2022).
63. M. Zamboni-Rached, "Stationary optical wave fields with arbitrary longitudinal shape by superposing equal frequency Bessel beams: Frozen Waves," Opt. Express **12**(17), 4001–4006 (2004).
64. T. A. Vieira, M. R. R. Gesualdi, and M. Zamboni-Rached, "Frozen waves: experimental generation," Opt. Lett. **37**(11), 2034–2036 (2012).
65. H. Zhou, X. Su, Y. Duan, *et al.*, "Atmospheric turbulence strength distribution along a propagation path probed by longitudinally structured optical beams," Nat. Commun. **14**(1), 4701 (2023).